Hindawi Publishing Corporation
International Journal of Antennas and Propagation
Volume 2014, Article ID 879127, 10 pages
http://dx.doi.org/10.1155/2014/879127

Research Article

A Single RF MIMO Loading Network for High-Order Modulation Schemes

Bo Han,[1,2] Vlasis I. Barousis,[1] Antonis Kalis,[3] Constantinos B. Papadias,[1] Athanasios G. Kanatas,[4] and Ramjee Prasad[2]

[1] *Athens Information Technology (AIT), Peania, 19002 Athens, Greece*
[2] *Center for TeleInFrastructur (CTIF), Aalborg University (AAU), 9220 Aalborg, Denmark*
[3] *SignalGeneriX, 59627 Limassol, Cyprus*
[4] *Department of Digital Systems, University of Piraeus, 18534 Piraeus, Greece*

Correspondence should be addressed to Bo Han; hab@es.aau.dk

Received 20 July 2013; Accepted 12 October 2013; Published 22 July 2014

Academic Editor: Demosthenes Vouyioukas

Recently, a novel MIMO transmitter architecture has been introduced that requires only a single radio-frequency (RF) chain and is built on parasitic antenna arrays. MIMO transmission in this case is achieved by shaping directly the radiation pattern with the aid of analog tunable loads attached to the parasitics. As it has been shown, such a single RF MIMO system can support all PSK modulation formats with purely imaginary loading values. This paper extends its capabilities and proposes a novel architecture for parasitic antennas that is able to provide *complex* loading values, even with a negative real part. Definitely, this will extend the flexibility of parasitic antennas to multiplex successfully over the air more complex signaling formats, for example, QAM signals. The bit error rate evaluation shows that the proposed architecture could be very promising in emerging devices and also illustrates its robustness under possible loading perturbations that might have been raised due to nonidealities in the design.

1. Introduction

The continuously increasing demand for higher data rates and reliable communication has excited the research interest to investigate novel MIMO architectures even for compact mobile devices. This is imposed by the considerable hardware complexity and the often bulkier dimensions of conventional MIMO architectures. Indeed, the existence of multiple radio-frequency (RF) chains hinders the wide deployment of conventional MIMO technology in mobile devices, mainly due to the additional hardware burden and power consumption. Another hindering factor is the correlation among the closely spaced antenna elements due to the strict size constraints. A variety of techniques have already dealt with the aforementioned problems. Indicatively, antenna selection algorithms [1, 2] select a subset of appropriate antenna elements to be connected to the available RF chains [3–5]. Although these techniques offer some complexity savings, often they cause significant performance degradation as compared to the conventional MIMO systems. Another approach known as antenna subarray formation applies mainly to the receiver's side and is based on the fundamental idea that every available RF chain is fed with a linear combination of the responses of a selected subset of antenna elements [6, 7]. Commonly, all those approaches cope with the problem of implementation complexity algorithmically, by activating appropriate antenna elements based on their responses. Another popular approach lies in antenna design and particularly on the investigation of novel multielement antenna configurations with strict size constraints [8].

An alternative perspective of MIMO technology, on which this paper focuses, was recently introduced [9–11]. This architecture is able to provide multiplexing over the air with a single RF chain and is known as single RF MIMO. Instead of the conventional trend of using arrays with multiple active elements, the proposed scheme is built on parasitic antenna arrays with a single active, that is, single feeding, port. Such antennas consist of an active element

surrounded by multiple parasitics in close proximity and are known as electronically steerable parasitic antenna radiators (ESPARs) [12, 13]. Due to the strong mutual electromagnetic coupling among all elements, the feeding of the active element induces strong currents to all parasitics. In this way, all parasitics participate in the radiation mechanism affecting the shape of the far field pattern. Further current control, or equivalently beam-shape control, is possible with the aid of low cost tunable analog circuits attached to all parasitic elements. Tuning those circuits, henceforth called loads, the effective coupling among all neighbor elements changes and this causes a corresponding change to all currents and consequently to the radiation pattern. It should be strongly emphasized that in applications with quite strict size constraints, for example, mobile devices, single RF MIMO often achieve even higher capacity performance as compared to their conventional counterparts with significant hardware complexity [14–16]. Therefore it is evident that single RF MIMO emerges as a novel and promising technology, able to bring the MIMO benefits to mobile devices. A proof-of-concept experiment of this architecture can be found in [17, 18]. Furthermore, the authors in [19] investigate an efficient methodology to enable multiplexing of 16-PSK symbols assuming *purely* imaginary loads. Those loads are realized with varactor diodes that are commonly used in ESPAR antenna designs. These components are a special kind of electronic diodes whose bias voltage controls their capacitance and thus they provide a tunable *pure* imaginary load.

However, the loading restriction to only imaginary values definitely limits the tuning capabilities of ESPAR antennas, implying that higher modulation schemes cannot be supported. Although it has been shown (both theoretically and experimentally) that MIMO is possible with a single RF chain, a challenging and persisting problem is the design of novel and low cost analog loading circuits that will be attached to the parasitics. This largely dictates the capability of ESPAR antennas to support higher modulation schemes as it will improve their beam-shaping abilities.

This is the main objective of this paper. In particular, this paper enables ESPAR antennas to multiplex high-order modulated signals, beyond PSK, over the air (e.g., QAM). This imposes the design of more sophisticated circuits, as compared to those in [19], which will provide *complex* loading with positive or negative real part. This in turn extends the capabilities of parasitic antennas and enables them to produce the required patterns, according to the single RF MIMO concept. We demonstrate the advanced loading flexibility of our approach using a simple 2-element ESPAR antenna, that is, a sole active element and a parasitic that is connected to the novel loading circuit. It is clearly shown that the proposed architecture succeeds to multiplex over the air multiple symbols emerging from a 16-QAM constellation, as it is able to produce the set of required radiation patterns.

This paper is organized as follows. Section 2 provides a brief description of the radiation characteristics of ESPAR antennas at the beamspace domain and also describes the procedure for determining all required loading values, given a certain modulation format. Sections 3 and 4 present in detail the functionality of the architecture that implements the required loading values for the parasitics. The performance of the proposed loading architecture and the consequent single RF MIMO transmitter is evaluated in terms of bit error rate in Section 5. Finally, Section 6 summarizes the key conclusions of the paper.

2. Beamspace Domain Representation of ESPAR Antennas

2.1. A Brief Review. As it is mentioned in Section 1, ESPAR antennas take advantage of the strong couplings among the elements and beamforming is possible by tuning the loading values that are attached to the parasitics. By doing so, the port currents change in a controllable manner. For a given current vector $\mathbf{i}$, the radiation pattern is

$$P(\vartheta,\varphi) = \mathbf{i}^T \mathbf{a}(\vartheta,\varphi) = \sum_{n=0}^{M-1} i_n a_n(\vartheta,\varphi), \tag{1}$$

where M is the number of ESPAR elements and $\mathbf{a}(\vartheta,\varphi)$ is the $(M\times 1)$ steering vector of the array. The $(M\times 1)$ current vector is related to the loading values as

$$\mathbf{i} = u_s(\mathbf{Z}+\mathbf{X})^{-1}\mathbf{v}. \tag{2}$$

In (2) $\mathbf{Z}$ is the $(M \times M)$ electromagnetic coupling matrix of the ESPAR antenna, $\mathbf{X} = \operatorname{diag}(R_s \;\; x_1 \;\; \cdots \;\; x_{M-1})$ is the load diagonal matrix that adjusts the radiation pattern, and R_s is the output impedance of the sole source impedance, while $\mathbf{v} = [1 \;\; 0 \;\; \cdots \;\; 0]^T$ is a $(M\times 1)$ selection vector and u_s is the feeding signal to the active port.

It is understood that in contrast to conventional multiport antenna arrays, ESPAR antennas do not offer spatial degrees of freedom (DoFs) as there exists a single active element. Thus, the conventional way of assigning multiple transmit symbols to different active elements is not applicable and at first glance MIMO communication is not possible. However, thanks to the tunable parasitics and the consequent beamforming abilities of ESPAR antennas, a vector of transmitted symbols can be encoded directly to a single radiation pattern. This functionality can be viewed clearly through the beamspace representation of ESPAR antennas, as explained in detail in [14–16]. According to that representation and considering without loss of generality propagation over the azimuth plane, that is, $\vartheta = \pi/2$, the radiation pattern of an ESPAR antenna given in (1) can be written as a linear combination of M basis patterns or aerial degrees of freedom (ADoFs) as

$$P(\varphi) = \sum_{n=0}^{M-1} w_n \Phi_n(\varphi). \tag{3}$$

It has been shown that the shape of all basis patterns depends on the interelement distance, while the coefficients w_n depend on the interelement distance and the currents (due to electromagnetic coupling the currents are also distance-dependent).

More details about the beamspace domain representation of ESPAR antennas can be found, for example, in [14] and the references therein.

Equation (3) reveals the functionality of the single RF MIMO transmitter: letting the coefficients be the complex symbols for transmission of an arbitrary signal constellation, (3) shows that M symbols have been attached, that is, mapped, to different basis patterns. Thus, symbols are not driven to diverse active antenna elements as in the conventional case, but they modulate orthogonal radiation patterns. In this way, at every symbol period the shape of the transmit pattern changes according to the symbol vector for transmission. Although this functionality looks very similar to beamforming, indeed it is a multiplexing operation defined at the beamspace domain. The ESPAR receiver in turn assesses the impinging signals by switching among orthogonal patterns within a symbol period [14]. A similar single RF receiver is proposed in [11]. Therefore, MIMO transmission so far has been emulated at the beamspace domain with single RF transceivers at both link ends. However, this paper focuses on the design of the single RF transmitter and therefore the bit error probability in Section 5 has been derived assuming a conventional MIMO receiver. It is also understood that the basis patterns in (3) remain orthogonal to each other as long as there is a reasonable amount of multipaths with different angles of departure. Otherwise, the radiation patterns are not sampled adequately in the angular domain and this will raise some amount of correlation among the basis patterns.

It should be strongly noted that although (3) implies that theoretically the number of symbols that can be multiplexed is equal to the number of all elements, [14, 15] mention that the interelement distance affects the *effective* number of ADoFs, that is, the number of basis patterns with significant contribution to the total radiated power that can practically be exploited for transmission. In this paper, an ESPAR antenna with $M = 2$ elements will be considered at 2.4 GHz, with a small interelement distance, where both basis patterns are strong and beam-shaping is possible [16].

2.2. Application to an ESPAR with 2 Elements. For an ESPAR antenna with $M = 2$ elements the basis patterns are given by [16]

$$\begin{aligned} \Phi_0(\varphi) &= \frac{1}{k_0}, \\ \Phi_1(\varphi) &= \frac{\left(e^{jb\cos\varphi} - 2\pi I_0(jb)/k_0^2\right)}{k_1}, \end{aligned} \tag{4}$$

where

$$\begin{aligned} k_0 &= \sqrt{2\pi}, \\ k_1 &= \sqrt{2\pi + \frac{\left(\pi/k_0^2 - 1\right) 8\pi^2 I_0^2(jb)}{k_0^2}}, \end{aligned} \tag{5}$$

and the coefficients in (3) are given by

$$\begin{aligned} w_0 &= i_0 k_0 + \frac{2\pi i_1 I_0(jb)}{k_0}, \\ w_1 &= i_1 k_1, \end{aligned} \tag{6}$$

where $b = 2\pi d$, d is the interelement distance normalized to wavelength, and $I_0(\cdot)$ is the zero-order modified Bessel function of the first kind. As it has been already stated, in case of small interelement spacing d, both basis patterns are strong and therefore multiplexing over the air is possible according to (3) [16]. Letting the coefficients in (6) be the complex symbols for transmission of an arbitrary signal constellation, it is evident that at each signaling period the desired symbol vector is produced by tuning the currents at the elements. This in turn can be achieved by adjusting appropriately the loading at the parasitic, as it will be explained next.

2.3. Loads Values for All Possible Symbol Vectors. A common assumption in the literature is that usually the tunable loads at the parasitic elements are implemented with varactor diodes, where their bias voltage controls the capacitance. Although this is a low cost implementation approach, often the pure imaginary load restricts the beam-shape abilities of the ESPAR antenna and thus the capability of the antenna to produce all the necessary radiation patterns dictated by (3). This fact becomes particularly evident as the constellation size becomes higher.

Although the authors in [19] succeed to encode any PSK modulated symbols onto the radiation patterns using purely imaginary loading, imposing a higher constellation, for example, QAM, imaginary loads can no longer produce the whole desired set of possible radiation patterns. To alleviate this problem, this section defines *complex* loading values that correspond to all possible transmit symbol vectors, or equivalently to all possible radiation patterns emerging from a 16-QAM modulation.

Recalling (3), when $M = 2$ the pattern becomes

$$P(\varphi) = w_0 \left(\Phi_0(\varphi) + \frac{w_1}{w_0} \Phi_1(\varphi) \right). \tag{7}$$

Equation (7) describes the triggering operation of the transmit ESPAR antenna. The first symbol w_0 is driven directly to the sole RF port, while the ratio w_1/w_0 determines the shape of the pattern. Therefore, the schematic of the single RF MIMO transmitter is the one depicted in Figure 1 that includes the ESPAR antenna and the triggering unit. At each signaling period a symbol vector $[w_0 \;\; w_1]$ is determined. Then, the tuning procedure maps the symbol ratio w_1/w_0 to a complex load x_1 that should be applied to the parasitic element, while the first symbol w_0 is fed to the active element. In this way the ESPAR is configured to the desired pattern and MIMO transmission is achieved as explained in Section 2.

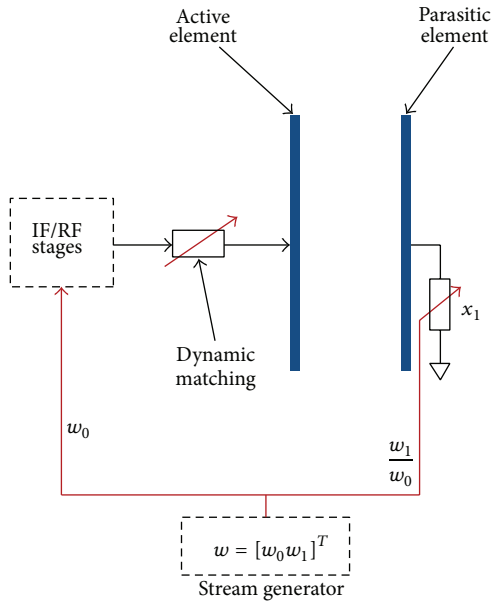

Figure 1: Topology of the proposed single RF MIMO transmission system.

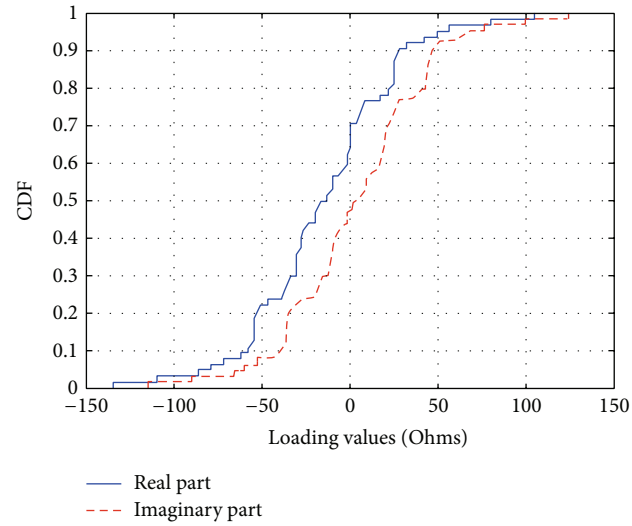

Figure 2: CDF pf the loading values that correspond to all possible 16-QAM symbol vectors.

In case of the ESPAR antenna with $M = 2$ elements, the transformation of the symbols to the load values are found by expanding (2) as

$$\left(\begin{bmatrix} Z_{11} & Z_{12} \\ Z_{21} & Z_{22} \end{bmatrix} + \begin{bmatrix} 50 & 0 \\ 0 & x_1 \end{bmatrix}\right)[i_0 \;\; i_1]^T = [u_s \;\; 0]^T. \quad (8)$$

From (8), and assuming $Z_{21} = Z_{12}$, we can get the required load value x_1 by

$$x_1 = -\left(\frac{i_0}{i_1} Z_{21} + Z_{22}\right). \quad (9)$$

According to (6), the above value can be rewritten as

$$x_1 = -\left(\left[\frac{w_0}{w_1} - \frac{2\pi I_0(jb)}{k_0 k_1}\right]\frac{k_1}{k_0} Z_{21} + Z_{22}\right), \quad (10)$$

where Z_{21} is mutual coupling of the two antenna elements. According to the constellation of the 16-QAM, there are totally 256 possible values of the ratio w_1/w_0. However, evaluating all of them, one observes that only 53 different loading values are required according to (10).

Figure 2 shows the cumulative distribution function (CDF) of the real and imaginary parts of the loads, as computed by (10), for all different 16-QAM transmit symbol vectors. It is mentioned that the mutual couplings in (10) are those that correspond to a real antenna design that is explained in Section 5. It is observed that the real part of the antenna load might be positive or negative. Therefore, if we were to take full advantage of the parasitic array capabilities, the loading circuit controlling the parasitic antenna loads should be able to provide a complex loading, which can be realized with a novel active circuit design. In this paper we describe such a design approach, which is the subject of the next sections.

3. Negative Resistance Circuit

3.1. System Level Requirement. From the aforementioned requirements, it is evident that an ESPAR antenna with 2 elements could multiplex two 16-QAM symbols given that the loading values are allowed to be complex with the real, that is, the resistive, part ranging from negative to positive values. Apparently, this can be achieved by replacing the varactor-based loading unit that has been used widely so far by a novel active circuit design. To emphasize this novel approach, hereafter the parasitic elements will be characterized as *active-loaded parasitics*.

To the authors' best knowledge, the idea of active-loaded parasitics has been first introduced in [20]. In particular, the main idea therein was to design a unit able to generate 4 negative values that are found to be appropriate for multiplexing two QPSK signals. Although in [20] along with the desired real part the proposed unit inevitably generates an imaginary component too, it has been found that this does not influence the performance, as long as an equivalent constellation could be defined. On the contrary, as the modulation format becomes more complex the number of the required loading states increases and a similar equivalent constellation cannot be found easily. Therefore, this paper proposes a universal (in the sense that the same topology could be used for designing a similar circuit that supports other modulation schemes or an arbitrary precoding) transmitter architecture with ESPAR antennas, comprised of active-loaded parasitic elements and a single RF chain. It will be shown that the proposed alternative is able to multiplex high-order modulation symbol formats over the air.

To achieve that goal, we propose the architecture shown in Figure 3. The active circuit in this figure is responsible to generate a *constant* negative resistance, which corresponds to the minimum value required for the given modulation scheme. To compensate the imaginary component of the active circuit and adjust the loading to the desired complex

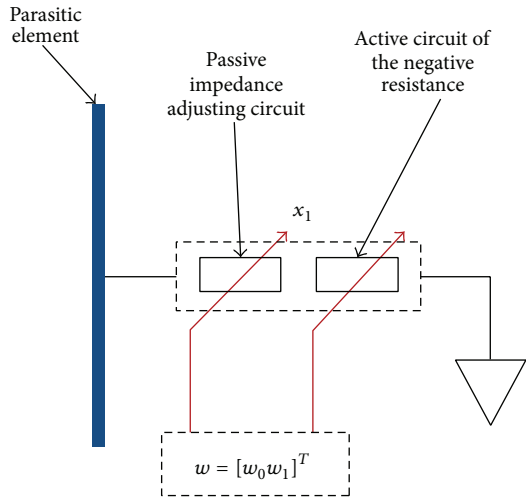

Figure 3: Topology of impedance control for the parasitic antenna.

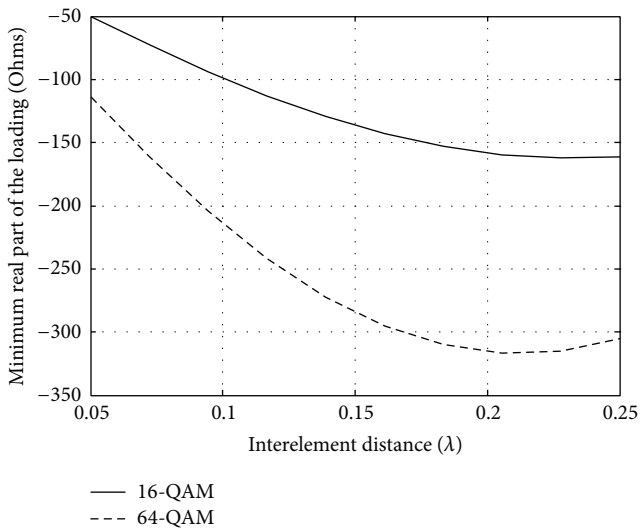

Figure 4: Minimum negative resistance value according to theory simulation.

value, a passive impedance adjusting circuit is also interpolated. In this way, the parasitic element is finally loaded with the desired complex loading value. In our design approach we initially estimate the lower bound of the loading. Recall that (10) gives the complex load as a function of the symbol ratio w_1/w_0 and the interelement distance d. Evaluating (10) for different interelement distances and assuming 16-QAM signaling one obtains Figure 4. In this figure, for each interelement distance all possible loading values are computed and the minimum one is plotted. As observed, the minimum value of x_1 is found to be below $-150\,\Omega$ for interelement spacings between $0.18\,\lambda$ and $0.25\,\lambda$. To provide a sense of the impact of the modulation order to the loading, Figure 4 includes also a curve that corresponds to the 64-QAM modulation scheme. Clearly, as the modulation scheme becomes more complex, the beam-shape requirements of the ESPAR become more demanding and this is reflected

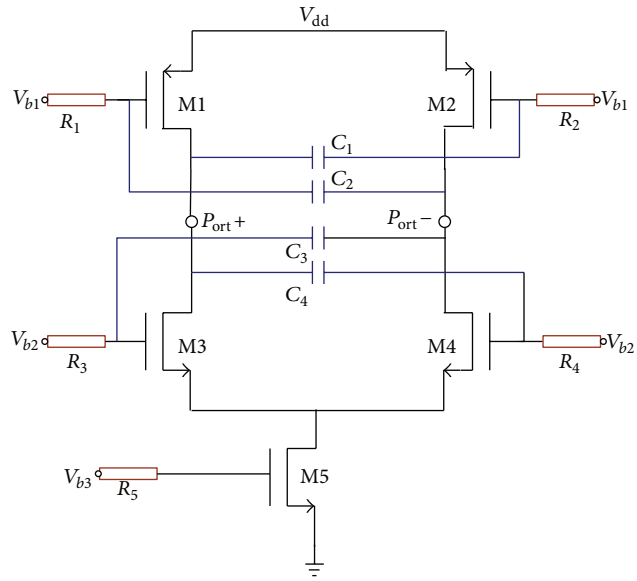

Figure 5: Negative resistance block using cross-coupling architecture.

to larger range of the required loading. It is noted that in this figure the mutual coupling between the two antenna elements is computed for each interelement distance using the theoretical formula presented in chapter 8 of [21]. Although this theoretical treatment assumes ideal dipoles in free space, it still provides a representative example of the dependence of the beam-shaping requirements with the modulation order. In Section 5, a realistic antenna design is assumed.

The simplest way to create an active circuit with tunable impedance is by using an operational amplifier (op-amp), which has a large open loop gain. However, commercial op-amps or low noise amplifiers (LNAs) usually provide a small open loop gain at high operating frequencies, for example, 1.9 GHz or 2.4 GHz. Taking also into account that usually such components are power hungry, they do not meet the low power requirements of mobile terminals. To satisfy the aforementioned constraints, next a novel circuit is described that is based on the complementary metal oxide semiconductor (CMOS) technology.

3.2. An Active Circuit Design for Generating Tunable Negative Resistance. Figure 5 shows the schematic of the proposed active circuit. The design is based on two cross-coupled transistor pairs under UMC 0.18 μm RF process. The PMOS transistors M1, M2 and the NMOS transistors M3, M4 are biased independently by voltages V_{b1}, V_{b2}, respectively. The individual biasing provides not only extra design flexibility, but also improved tuning capability. The NMOS transistor M5 works as a current source and it is designed with enlarged width W and length L to reduce the flicker noise. The DC-biasing components $R_1 - R_4$ are resistors with high value to provide isolation from the circuit that sets the biased voltages. The circuit is powered by $V_{dd} = 1.2$ V, which is a trend in portable applications. The tunable resistance is measured

between the ports $P_{\text{ort}}+$ and $P_{\text{ort}}-$ in Figure 5 and is given by the following equation [22]:

$$R_{\text{neg}} = \frac{-1}{\left(g_{mn} + g_{mp}\right)} = -\frac{V_{\text{gs}} - V_{\text{th}}}{2I_{\text{ds}}} = \frac{-\left(u_n + u_p\right)L}{u_n u_p C_{\text{ox}} W \left(V_{\text{gs}} - V_{\text{th}}\right)} = -\sqrt{\frac{\left(u_n + u_p\right)2n}{u_n u_p C_{\text{ox}}} \frac{L}{W} \frac{1}{4I_{\text{ds}}}}, \tag{11}$$

where g_{mn}, g_{mp} are the transconductances of NMOS transistor and PMOS transistor respectively, expressed as

$$g_{m(n,p)} = u_{(n,p)} C_{\text{ox}} \frac{W}{L} \left(V_{\text{gs}} - V_{\text{th}}\right) = 2\frac{I_{\text{ds}}}{V_{\text{gs}} - V_{\text{th}}}. \tag{12}$$

Moreover, $\mu_{(n,p)}C_{\text{ox}}$ is a process related coefficient, W/L is the ratio of channel width and channel length of the transistor, I_{ds} is the current flowing though the transistor, V_{gs} is the voltage between gate and source, and V_{th} is the threshold voltage of the transistor. The smaller the current I_{ds}, the smaller the negative resistance we get. In submicrometer processes, the effect of the channel length should be taken into consideration and therefore [22]

$$I_{\text{ds}} = \frac{u_n u_p C_{\text{ox}}}{2\left(u_n + u_p\right)} \frac{W}{L} \left(V_{\text{gs}} - V_{\text{th}}\right)^2 \left(1 + \lambda_{\text{tr}} V_{\text{ds}}\right), \qquad R_{\text{neg}} = \frac{-\left(u_n + u_p\right)L}{u_n u_p C_{\text{ox}} W \left(V_{\text{gs}} - V_{\text{th}}\right)\left(1 + \lambda_{\text{tr}} V_{\text{ds}}\right)}, \tag{13}$$

where λ_{tr} is the coefficient related to the effect of the channels length and V_{ds} is the voltage between the source and drain of the transistor.

3.3. Simulated Negative Resistance Values. Based on the aforementioned theoretical analysis, we set the size of the transistors M1 and M2 to $W/L = 10/0.18$. Regarding the transistors M3 and M4 this value is set to $W/L = 45/0.18$, while the current source M5 operates with a bias current of 1 mA. The capacitors C1–C4 are set to 1 pF and the resistors $R_1 - R_4$ are 1 MΩ. The active circuit in Figure 5 has been characterized by the S parameters obtained in Advanced Design System (ADS) software, which is an electronic design software for RF, microwave, and high speed digital applications. Based on this design setup, a fixed negative resistance value is selected by setting appropriately the bias voltages. This value is shown in Figure 6 obtained in ADS as a function of frequency. The horizontal axis is the frequency in GHz and vertical axis is the impedance value in Ω. Two markers indicate the real and imaginary parts of the impedance, respectively. According to the simulation, the real part of the impedance below 2.5 GHz is found smaller than −230.6 Ω and the imaginary part smaller than −117.9 Ω. It is noted that for the selected frequency of operation at 2.4 GHz (see Section 5),

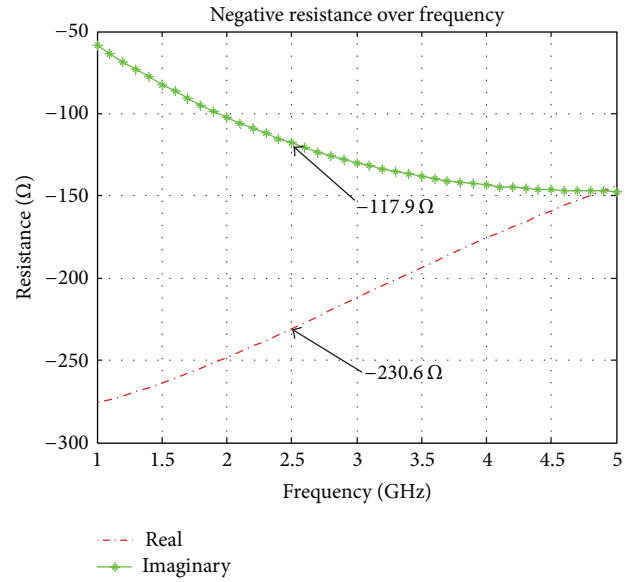

Figure 6: Simulated negative resistance values.

the corresponding impedance is finally adjusted to the desired loading by the impedance matching network presented at the next section. Compared with the loading requirements drawn in Figure 2, the result of the proposed negative resistance unit is more than sufficient. It is mentioned that as every active circuit, this also requires an external power supply that will provide the necessary biasing. However, the underlying power consumption is negligible as it has been found in [20] to be at the order of microwatts. Therefore, the design and the proposed architecture still remain energy efficient.

4. Loading Switching

4.1. Adjusting Stages. According to the proposed circuit architecture shown in Figure 2, in order to compensate with the imaginary component of the active circuit and adjust the load to the desired value, a switching passive impedance matching grid should be included. The adjusting unit is composed of 53 discrete values that are equal to the unique loading values as indicated in (10), where each one contains resistive R_{adj} and inductive L_{adj} components. As shown in Figure 7 the proposed adjusting unit consists of an 8 × 8 array and two 3-to-8 converters (although an 7 × 8 array with 3 redundant cells could be used, a 3-to-7 converter is not available widely in the market). The cells of this array hold 53 discrete values, while the remaining ones are unused. CMOS Port 1 is connected to the ports of the negative resistance circuit described in Figure 5, and the RF Port 2 is connected to the parasitic antenna. In this topology, only 6 control bits are required to select one out of the 53 values. Based on this implementation approach, each symbol vector is mapped to a 6-bit code-word and at each signaling period the appropriate one applies to retrieve the correct value of the load matrix. An example of such a selection is shown in Figure 7.

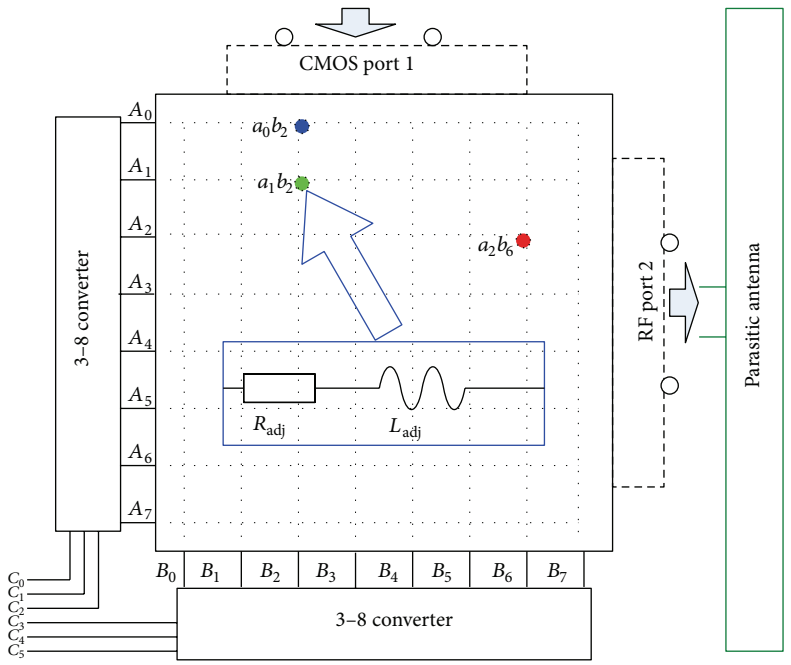

Figure 7: Topology of the proposed digitally controlled adjusting network.

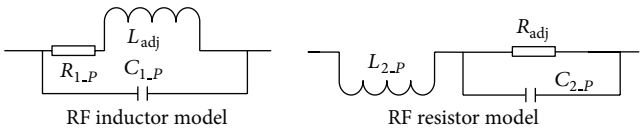

Figure 8: Small circuit model of resistor and inductor at high frequency.

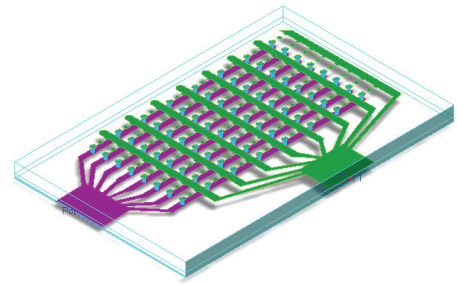

Figure 9: 3D view of the proposed load switching array produced in ADS design software.

It should be noted however that the proposed solution assumes instantaneous transitions between consecutive loading states. Although in practical designs the switching speed can be at the order of nanoseconds, in a real system the transmitted signal must satisfy specific bandwidth constraints. Therefore, a smoother and controllable transition between different loading states is needed. However, this issue deserves further study and is out of the scope of this paper.

4.2. Performance and Tolerance Simulation. Although we have a way to define the required loading values, at high frequencies additional nonidealities due to parasitic effects have to be also considered, as indicated in Figure 8 [23]. According to that figure, the impedance of the resistor and the inductor including the parasitic effects is given by

$$Z_{\text{res}} = j\omega L_{2\_P} + \frac{1}{j\omega C_{2\_P} + 1/R_2},$$
$$Z_{\text{ind}} = \frac{j\omega L_1 + R_{1\_P}}{1 + j\omega C_{1\_P}\left(R_{1\_P} + j\omega L_1\right)}. \quad (14)$$

The practical nonidealities that count not only for the parasitic effects but also for the mounting pad influence have been simulated in ADS. For completeness, the resulting model as obtained in ADS is shown in Figure 9. Taking into account this model, we observed a variation from the desired values in the order of around 2.5 Ω. Similar variations have been also reported in the literature, for example, [23]. It is noted that this deviation is representative for all loading states. It should be worthy to note that the adjusting matching network in Figure 7 has been proposed as an easy-to-implement solution, with fixed and predefined impedance values. Applying a deembedding technique (e.g., [24, 25]), one could easily compensate possible parasitic effects during the design procedure by taking them into account and optimizing the final impedance values on the grid. Therefore, it is understood that the treatment of the parasitic effects, at least to some extent, is a matter of implementation. In Section 5, however, we illustrate the impact of possible loading perturbations that might be present on the performance in terms of bit error probability.

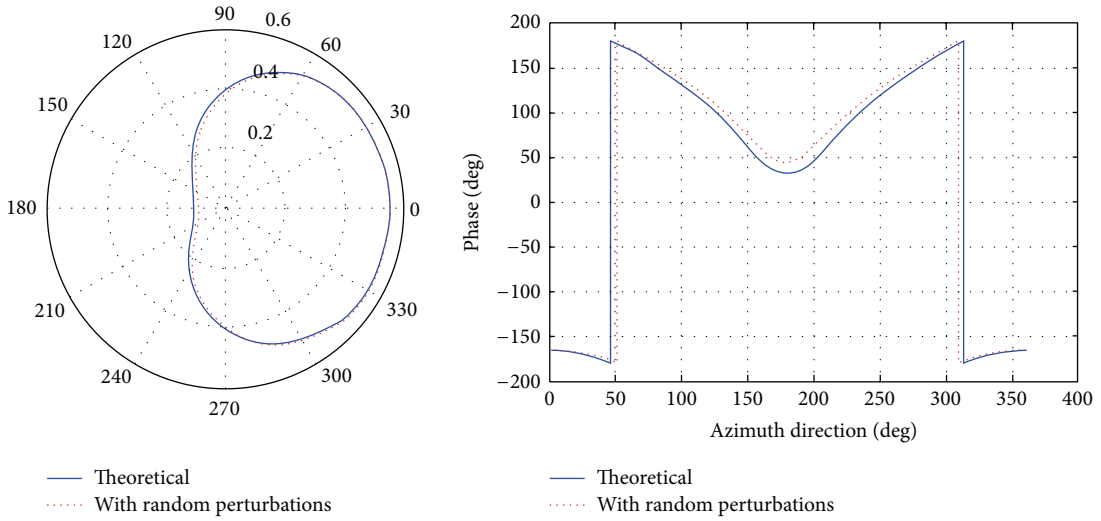

Figure 10: Theoretical and practical radiation patterns gains and phase.

5. Performance Evaluation

The performance of the proposed single-RF MIMO architecture is evaluated with a realistic ESPAR antenna, which has been designed in IE3D (this is a full-wave, method-of-moments based electromagnetic simulator solving the current distribution on 3D and multilayer structures of general shape and is provided by Mentor Graphics) using a metal thickness of 0.0254 mm and an FR4 substrate with thickness of 1.6 mm and dielectric constant of $E_r = 4.45$. The active element is selected as a folded-dipole, while the parasitic is a conventional dipole, while their interelement spacing is selected as $d \approx 0.23\,\lambda_{\text{eff}}$, $\lambda_{\text{eff}} = \lambda_0/\sqrt{E_r}$, where λ_0 is the wavelength in vacuum, that is, 125 mm at 2.4 GHz. The existence of small perturbations due to nonidealities on the loading states might change the shape of the desired pattern given in (3). Indicatively, Figure 10 shows a comparison between a desired pattern, that is, the theoretical, and the corresponding one with an extra deviation at the real and imaginary parts of the loading that represents the effect of nonidealities. As observed, both patterns are very identical, especially regarding the amplitude component. This high accuracy is achieved in all cases.

Figure 11 offers a valuable comparison of the bit error probability when a conventional zero-forcing receiver with two antenna elements is utilized and the ESPAR antenna at the transmitter (as described in Figure 1) multiplexes two 16-QAM signals. As observed, the performance using the theoretical loading values is compared against the case of two different ranges of loading deviation, that is, 3 and 4 Ohms (i.e., more than the one found with ADS), which model any possible and inevitable nonidealities. Reasonably, the loading deviations change slightly the currents at the ports of the ESPAR elements and in turn the actual signal constellation. Consequently, this causes a performance degradation in high E_b/N_o regime, but since it is expected that the mobile devices in future wireless systems will operate in the low E_b/N_o regime, the system remains robust and those nonidealities can be ignored.

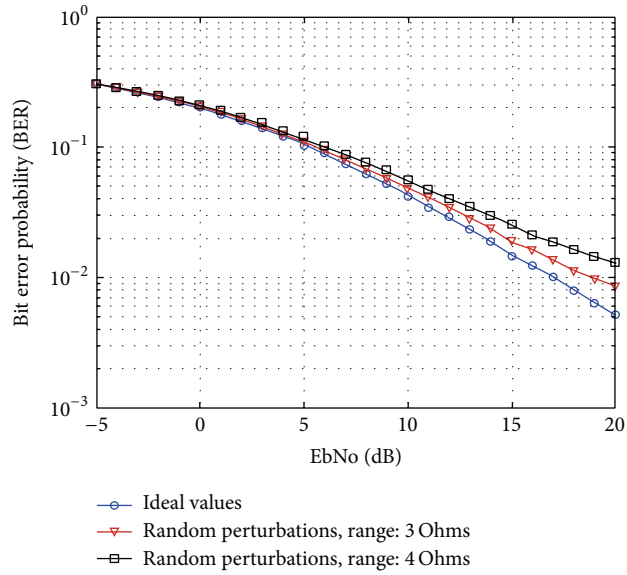

Figure 11: Bit error probability performance, under various loading conditions.

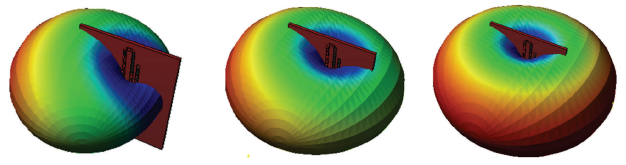

Figure 12: Three indicative radiation patterns obtained from IE3D.

Eventually, the end-to-end performance could be further improved by using more robust receiving techniques such as ordered successive cancellation (OSUC) zero-forcing, or even more complex ones [26]. For completeness, Figure 12 illustrates 3D examples of radiation patterns obtained in IE3D

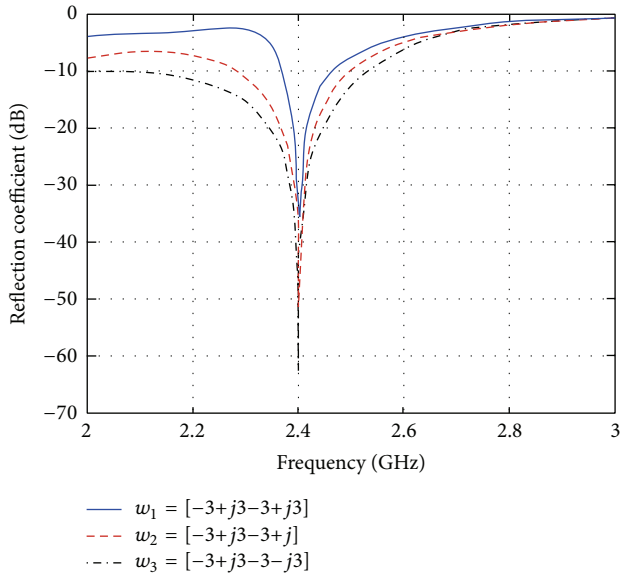

FIGURE 13: Simulated indicative return loss of the first 16 load values.

software, where each of them corresponds to a different 16-QAM symbol vector for transmission. Also, Figure 13 shows the return losses of the antenna for each of the patterns in Figure 12, as they are computed in IE3D antenna design software. As expected, the curve of the return loss for a certain pattern is different, since it depends on the loading values. Clearly, at 2.4 GHz the reflection coefficient is almost zero, as expected. As it has been verified, the same trend applies for all possible radiation patterns.

6. Conclusion

This paper presents a novel loading architecture that supports a reliable MIMO transmission with the aid of a single RF chain and a parasitic antenna array with closely spaced elements. Instead of the conventional trend of using purely imaginary loads, complex loading values with positive or negative real part are generated via an active circuit design. The consequent additional flexibility is found to improve significantly the beam-shaping abilities of the parasitic antenna, which as it has been shown succeeds to multiplex 16-QAM signals over the air. Therefore, MIMO transmission is emulated with a single RF chain. The remarkable hardware savings and the reduced antenna dimensions constitute the proposed architecture a strong candidate for battery-charged and lightweight devices. Although this architecture is demonstrated for 16-QAM signals, clearly the same design procedure can be used to support an arbitrary signaling format, an arbitrary precoding scheme, or power control policy.

Conflict of Interests

The authors declare that there is no conflict of interests regarding the publication of this paper.

Acknowledgments

The authors acknowledge the valuable contribution of Mr. Eleftherios Roumpakias, who is a Research Engineer in Broadband Wireless Sensor Networks (B-WiSE) Lab at Athens Information Technology (AIT), Greece. This work is supported by European Commission Founded SmartEN (Grant no. 238726) Marie Curie ITN FP7 Program. This work is also supported under the collaboration between Aalborg University and Athens Information Technology.

References

[1] A. Gorokhov, D. A. Gore, and A. J. Paulraj, "Receive antenna selection for MIMO spatial multiplexing: theory and algorithms," *IEEE Transactions on Signal Processing*, vol. 51, no. 11, pp. 2796–2807, 2003.

[2] A. Gorokhov, D. Gore, and A. Paulraj, "Receive antenna selection for MIMO flat-fading channels: theory and algorithms," *IEEE Transactions on Information Theory*, vol. 49, no. 10, pp. 2687–2696, 2003.

[3] P. D. Karamalis, N. D. Skentos, and A. G. Kanatas, "Selecting array configurations for MIMO systems: an evolutionary computation approach," *IEEE Transactions on Wireless Communications*, vol. 3, no. 6, pp. 1994–1998, 2004.

[4] D. A. Gore and A. J. Paulraj, "MIMO antenna subset selection with space-time coding," *IEEE Transactions on Signal Processing*, vol. 50, no. 10, pp. 2580–2588, 2002.

[5] P. J. Voltz, "Characterization of the optimum transmitter correlation matrix for MIMO with antenna subset selection," *IEEE Transactions on Communications*, vol. 51, no. 11, pp. 1779–1782, 2003.

[6] P. Theofilakos and A. G. Kanatas, "Capacity performance of adaptive receive antenna subarray formation for MIMO systems," *EURASIP Journal on Wireless Communications and Networking*, vol. 2007, Article ID 56471, 2007.

[7] P. Theofilakos and A. G. Kanatas, "Maximising capacity of MIMO systems with receive antenna subarray formation," *Electronics Letters*, vol. 44, no. 20, pp. 1204–1206, 2008.

[8] J. Villanen, P. Suvikunnas, C. Icheln, J. Ollikainen, and P. Vainikainen, "Performance analysis and design aspects of mobile-terminal multiantenna configurations," *IEEE Transactions on Vehicular Technology*, vol. 57, no. 3, pp. 1664–1674, 2008.

[9] A. Kalis, A. G. Kanatas, and C. B. Papadias, "A novel approach to MIMO transmission using a single RF front end," *IEEE Journal on Selected Areas in Communications*, vol. 26, no. 6, pp. 972–980, 2008.

[10] A. Kalis and C. Papadias, "An ESPAR antenna for beamspace-MIMO systems using PSK modulation schemes," in *Proceedings of the IEEE International Conference on Communications (ICC '07)*, pp. 5348–5353, June 2007.

[11] R. Bains and R. R. Müller, "Using parasitic elements for implementing the rotating antenna for MIMO receivers," *IEEE Transactions on Wireless Communications*, vol. 7, no. 11, pp. 4522–4533, 2008.

[12] R. F. Harrington, "Reactively controlled directive arrays," *IEEE Transactions on Antennas and Propagation*, vol. 26, no. 3, pp. 390–395, 1978.

[13] C. Sun, A. Hirata, T. Ohira, and N. C. Karmakar, "Fast beamforming of electronically steerable parasitic array radiator antennas: theory and experiment," *IEEE Transactions on Antennas and Propagation*, vol. 52, no. 7, pp. 1819–1832, 2004.

[14] V. I. Barousis, A. G. Kanatas, and A. Kalis, "Beamspace-domain analysis of single-RF front-end MIMO systems," *IEEE Transactions on Vehicular Technology*, vol. 60, no. 3, pp. 1195–1199, 2011.

[15] V. I. Barousis and A. G. Kanatas, "Aerial degrees of freedom of parasitic arrays for single RF front end MIMO receivers," *Progress in Electromagnetics Research B*, vol. 35, pp. 287–306, 2011.

[16] V. Barousis, A. Kalis, and A. G. Kanatas, "Single RF MIMO systems: exploiting the capabilities of parasitic antennas," in *Proceedings of the 74th IEEE Vehicular Technology Conference (VTC-Fall '11)*, pp. 5–8, September 2011.

[17] O. N. Alrabadi, J. Perruisseau-Carrier, and A. Kalis, "MIMO transmission using a single RF source: theory and antenna design," *IEEE Transactions on Antennas and Propagation*, vol. 60, no. 2, pp. 654–664, 2012.

[18] O. N. Alrabadi, C. Divarathne, P. Tragas et al., "Spatial multiplexing with a single radio: proof-of-concept experiments in an indoor environment with a 2.6-GHz prototype," *IEEE Communications Letters*, vol. 15, no. 2, pp. 178–180, 2011.

[19] O. N. Alrabadi, C. B. Papadias, A. Kalis, and R. Prasad, "A universal encoding scheme for MIMO transmission using a single active element for PSK modulation schemes," *IEEE Transactions on Wireless Communications*, vol. 8, no. 10, pp. 5133–5142, 2009.

[20] B. Han, V. Barousis, A. Kalis, and A. G. Kanatas, "Active parasitic arrays for low cost compact MIMO transmitters," in *Proceedings of the IEEE 5th European Conference on Antennas and Propagation (EUCAP '11)*, vol. 1, pp. 3663–3667, April 2011.

[21] C. Balanis, *Antenna Theory, Analysis and Design*, John Wiley & Sons, 2005.

[22] B. Razavi, *RF Microelectronics*, Prentice Hall, 1998.

[23] C. Bowick, J. Blyer, and C. Ajluni, *RF Circuit Design*, Newnes Elsevier, 2008.

[24] B. Han, M. Liu, and N. Ge, "A UWB down convert circuit and measurement," in *Proceedings of the IEEE International Conference on Microwave and Millimeter Wave Technology (ICMMT '10)*, vol. 1, pp. 1472–1475, May 2010.

[25] T. Hirano, J. Hirokawa, M. Ando, H. Nakano, and Y. Hirachi, "De-embedding of lumped-element characteristics with the aid of EM analysis," in *Proceedings of the IEEE International Symposium on Antennas and Propagation Society (AP-S '08)*, vol. 1, pp. 1–4, July 2008.

[26] A. Paulraj, R. Nabar, and D. Gore, *Introduction To Space-Time Wireless Communications*, Combridge University Press, 2003.